Predicting Embryonic Dynamics and Development with a Diffusion-Based Model of Micro-CT Image Studies

BEE 4530

Miles Francken, Levi Patish, David Streitman, Sho Yoshitake

Table of Contents

1. Executive Summary

Although the chick embryo has long been used as a model for mammalian embryogenesis, there is a need to understand the changing tissue properties that cause physiological changes. Most imaging techniques have proven inadequate for real-time *in vivo* imaging of soft tissues. However, Micro-CT technology with gold nanoparticles as contrast agents can be used as an alternative. These nanoparticles readily dissolve into soft tissues and thus mitigate the need to fix samples (Murphy et.al, 2008). Using X-rays to excite these nanoparticles produces 2-D image slices, which can then be combined to create a complete 3-D image.

In this study, this imaging technique was coupled with computational modeling to determine the dynamics of tissue properties in chick embryos. Gold nanoparticles were injected into chick embryos, and Micro-CT images were taken at various time points within 24 hours following injection. A novel image analysis technique was then developed and used to quantify the accumulation of the nanoparticles in the myocardial tissue directly from the images. The heart and surrounding pericardial cavity were isolated and approximated as a sphere with a semi-aqueous layer surrounding the sphere, respectively. Using this geometry, a 1-D radially axisymmetric diffusion model was created in COMSOL. A function for diffusivity of nanoparticle in myocardial tissue as well as partition coefficient in the heart lumen were found by minimizing the discrepancy between the model and experimental values.

Although the experimental results followed expectations, the model did not match the results. As expected, there was accumulation of nanoparticle in the myocardial tissue, and the rate of this accumulation decreased with time. Optimization of the model yielded a diffusivity function and partition coefficient of $D_a = 1.0 * 10^{-14} e^{-10^{-7} t}$ and 80, respectively. But, these values corresponded to a total discrepancy of 29.94 %. This difference could be attributed to variability in the image processing methods or the computational model.

However, analysis of the image processing methods showed robustness and reliability. When three group members independently analyzed ten images, the difference in total mass was less than 5%. Consequently, the contribution of each parameter on the discrepancy was resolved.

This was done by performing sensitivity analyses on the parameters. From this, it was clear that, for the diffusivity function of the nanoparticle in the myocardial tissue, the initial diffusivity had a much larger impact on the total discrepancy than the rate of decay. Furthermore, the partition coefficient had a large impact on the total discrepancy. However, the total discrepancy did not differ greatly for values similar to the optimal values. From this, it was evident that changing these parameters would not lead to a lower difference; the study needed to be improved. Possible enhancements include including more experimental data and connecting the heart to other organs in the model, among others.

2. Introduction

The chick embryo has long been used as a model for mammalian embryogenesis. In general, embryogenesis consists of growth, differentiation and organization events (DeHaan et.al, 1964). Chick embryo development lasts around 21 days and can be split into 46 distinct morphological stages (Hamburger and Hamilton, 1951). These phases have been identified using differentiation events, such as notochord development, the number of pairs of somites, and limb growth as markers.

Although this characterization scheme has been essential for creating a clear framework for identifying embryos, the physiological events connecting each phase remain unclear. Various imaging techniques have been used in order to bridge these gaps. These include optical imaging, ultrasound, magnetic resonance imaging (MRI) and micro-computed tomography (micro-CT). While optical imaging has been helpful in generating more detailed images of cell and matrix movements, its resolution is limited by diffraction in many cases and cannot be done in vivo (Gregg and Butcher, 2012). Ultrasound imaging has been used to derive real-time information about blood flow in embryos (Gregg and Butcher, 2012). However, the contrast agents that have been used are microbubbles that are injected intravenously and stay in circulation, preventing analysis of tissue properties. MRI can be used to derive these properties in real-time without the addition of contrast agents, but it requires long scan times ranging from 6 to 24 hours (Gregg and Butcher, 2012). Consequently, changes within phases cannot be distinguished.

Micro-CT technology is an alternative to these imaging techniques and can be used to provide real-time *in vivo* imaging. This technology utilizes X-rays to cause emission of gamma particles in samples. This produces 2-D image slices that can be combined to create a 3-D image. It is possible to image soft tissue with this technology through the use of contrast agents. However, common contrast agents require fixation of the sample (Gregg and Butcher 2012). Recently, it has been shown that gold nanoparticles can be used as a non-invasive substitute (Murphy et.al, 2008). Gold nanoparticles have been used with Micro-CT technology to visualize tumors and tissues in real time (Hainfeld et al., 2012; Reuveni et al., 2011). However, tissue properties have not been ascertained from image data. Furthermore, quantification of nanoparticle accumulation has only been performed *ex vivo* (Hainfeld et al., 2014).

In order to obtain tissue property dynamics of a chick embryo from Micro-CT technology with gold nanoparticles, experimental analysis was coupled with computational modeling. Gold nanoparticles were injected into a chick embryo between day 7 and 8 of incubation, equivalent to stages 29 to 31 in development (Hamburger and Hamilton, 1951), and images were taken at various times during this period. A novel image analysis method was developed to quantify the accumulation of gold nanoparticles in myocardial tissue at these times. COMSOL was then used to determine the dynamics of the partition coefficient between the heart lumen and tissue as well as the diffusivity of the myocardial tissue.

3. Problem Statement

Micro-CT technology with gold nanoparticles as contrast agents can provide real-time *in vivo* imaging of chick embryo hearts. But, computational modeling is necessary to equate the accumulation of the nanoparticles into the myocardial tissue with changing tissue properties. The purpose of our project is to use a computer-based model in COMSOL to accurately predict the diffusive dynamics of developing chick embryo tissue and the corresponding changes in tissue material properties over time, such as diffusivity and porosity.

4. Design Objectives

- To create a diffusive model describing fundamental movement of nanoparticles
- To extract information about changes in material properties over time
- To resolve contributions of each computational parameter in the overall diffusion model

5. Model Design

For a summary of all governing equations and computational parameters used in the design of this model, please refer to the information outlined in Appendix A.

5.1 Computational Domain

In order to capture the diffusion dynamics within the chick embryo heart, we modeled this developing organ as a sphere in COMSOL, framing it as a 1D axisymmetric geometry due to radial symmetry. The model consists of a spherical tissue layer with outer radius r_2 and inner radius r_1 surrounding a control volume of blood: the chamber of the heart. The geometry will be axisymmetric about the *z* axis, limiting diffusion to radial progression from the inner heart chamber boundary through the myocardial tissue layer. Surrounding this myocardium volume is a complex matrix of developing tissue, which for the purposes of this model has been approximated as an aqueous environment which will allow for continued diffusion in water. This ‘pericardial cavity’ is concurrent with the myocardial tissue, and is defined by an outer radius, denoted as r_3.

Based on experimental parameters collected by Kim *et al*., the following heart dimensions were gathered:

Table 1. *Tabulation of myocardial dimensions over 24 hour interval of analysis.*

Day	Total Heart Volume (mm^3)	r_2 (mm)	Chamber Volume (mm^3)	r_1 (mm)	Tissue Thickness (mm)
7 *(0 hours)*	12.90	1.45	10.85	1.37	0.080
8 *(24 hours)*	16.87	1.59	12.48	1.44	0.15

Using additional regression data from Kim *et al*., we approximated a linear relationship to model the time-dependent growth of the computational domain, and incorporated this into our model using a moving boundary geometry element. This will be modeled with the velocity approximated as a linear progression of growth over the 24 hour period, as shown below,

$$v_i = \frac{r_{i_{final}} - r_{i_{initial}}}{24\ hours} \tag{1}$$

where i = 1 for the heart chamber wall and i = 2 for the outer myocardial tissue wall. It is assumed that maintaining the pseudo-aqueous computational domain as a fixed scalar multiple of the tissue thickness be preserve the semi-infinite approximation as both the heart chamber and tissue domains grow over time. A general schematic summarizing the geometry and computational domain as implemented in COMSOL is provided in Figure 1.

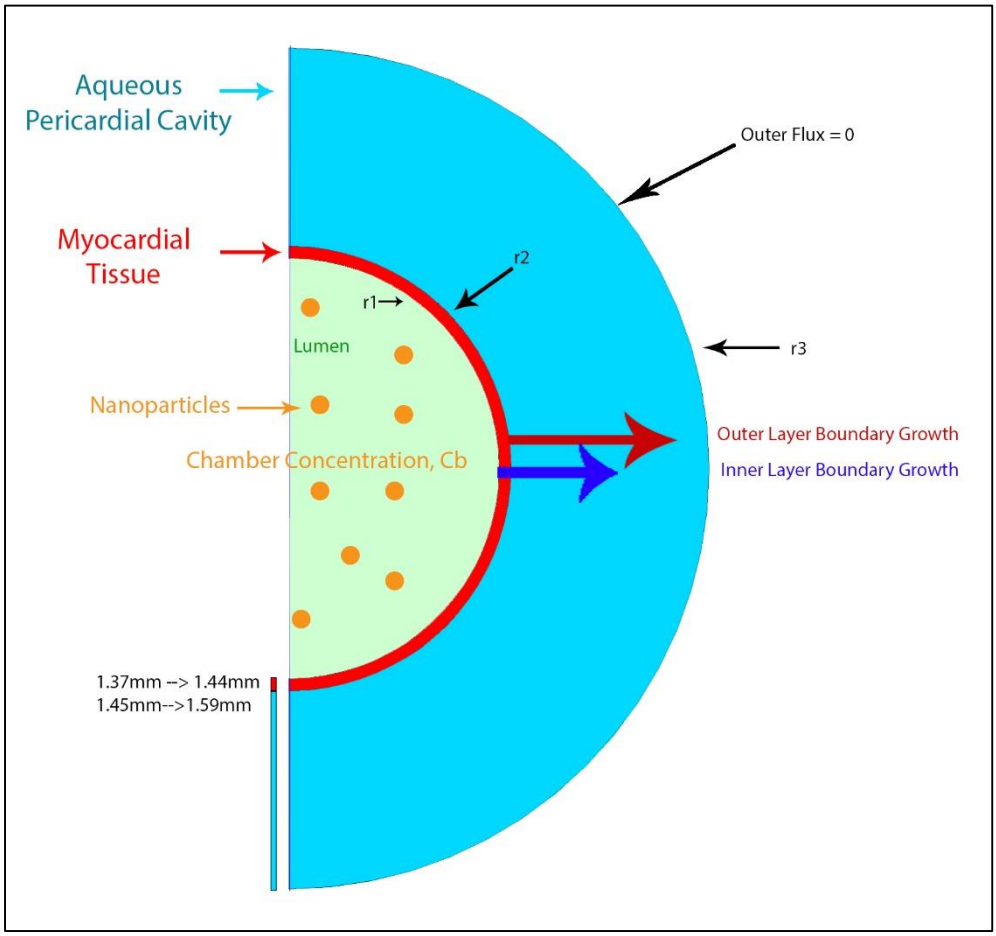

Figure 1. *Schematic of 1D radial diffusion of nanoparticles in embryonic myocardium***.** Shown above is a simplified schematic of the governing geometry and boundary conditions for the diffusion of radiopaque nanoparticles into the chick embryonic tissue**.**

5.2 Assumptions

Due to the rapid flow of blood in the systemic circulation of the embryo, the concentration of nanoparticles in the systemic circulation was assumed to be homogenous throughout the entire blood volume at any given time, allowing for the removal of diffusion dependence in the φ or θ directions. Furthermore, the dynamics of the system was simulated over a 24 hour period following an initial injection of nanoparticles into the circulation. Several complexities will be tackled in this modeling process due to the large changes undergone by the embryo in both structure and material properties. Primarily, we expect the tissue to experience a decrease in overall porosity as cells become differentiated and organize themselves into higher order structures, causing the diffusive properties of the tissue to change with time. Furthermore, the increase in the overall size of the embryo during growth causes an increase in the blood circulation volume, invariably diluting the initial injected mass of nanoparticles over time. The specific time-dependent data used in this

approximation was taken from experimental data by Kind *et al.*, and a summary of this data is presented below in Figure 2.

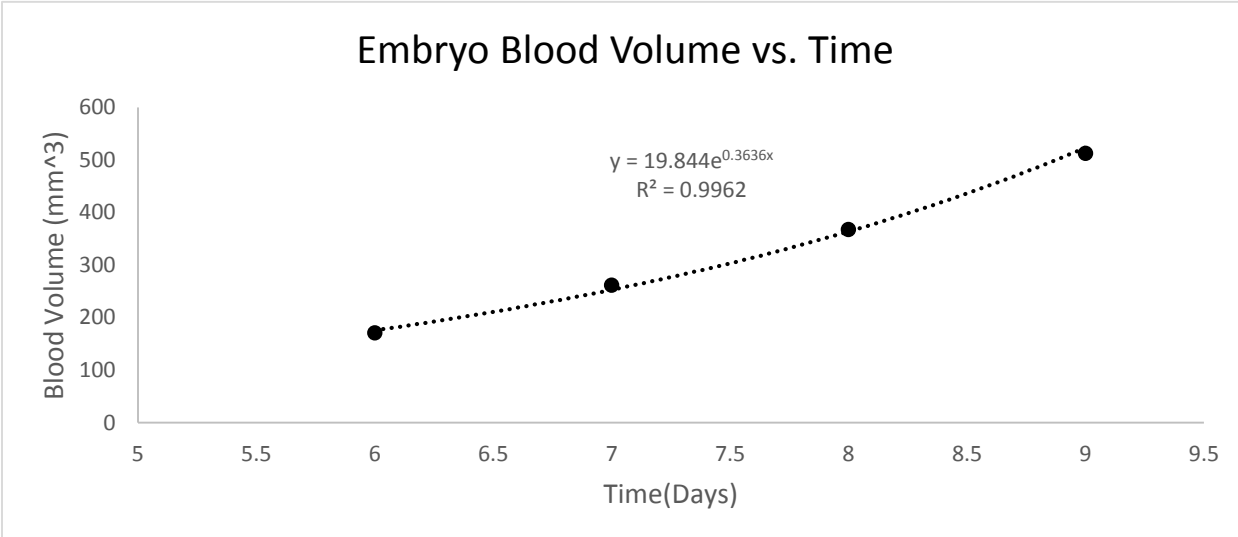

Figure 2. *Best-Fit Exponential Curve for Blood Volume (mm^3) vs. Time (hrs*). Using the mean blood volumes from day 6 to day 9 (Kind 1975), an exponential regression was developed to approximate changes in total blood volume

5.3 Governing Equation

The following equation is the simplified form of the general mass transfer equation for a species in 1D axisymmetric cylindrical coordinates,

$$\frac{\partial c_a}{\partial t} = \frac{D_a(t)}{r^2}\frac{\partial}{\partial r}\left[r^2\frac{\partial c_a}{\partial r}\right] \tag{2}$$

where c_a is the concentration of radiopaque nanoparticles in the embryonic tissue, D_a is the effective diffusivity of these particles within the tissue, and r is the radial distance from the center of the heart chamber. In this equation, the governing terms for convection and metabolism have been removed because we ignored bulk transport effects as well as any potential sequestration or degradation of the nanoparticles over the duration of simulation. Diffusive dependence in the φ or θ coordinate directions was neglected due to the 1D axisymmetric assumption previously stated for the computational domain.

Additionally, the diffusivity of the tissue was approximated as a time-dependent expression to capture the growth and differentiation of heart tissue as the chick develops:

$$D_a = Ae^{-Bt} \tag{3}$$

Consultation with a subject matter expert consequently deemed this negative exponential fit was appropriate to model this phenomena based on a qualitative understanding of the change in tissue structure complexity over time. The parameters A and B were subsequently subjected to a parametric sweep in COMSOL to adjust the dynamics of the model to better simulate the actual movement of nanoparticles observed in experimentation. It has further been assumed that the diffusivity will preserve spatial uniformity throughout the computational domain, based on the reasoning that, within this length scale, the tissue can essentially be considered uniform and is differentiating homogenously.

5.4 Boundary Conditions

To specify the governing equation presented above, two spatial boundary conditions are required, and these are summarized as follows:

1) **At the boundary $\boldsymbol{r = r_1}$**, a concentration condition was used that was equal to the concentration of nanoparticles in the lumen of the heart. This value was determined based on a mass balance between the heart chamber and the tissue domain,

$$C_b(t) = K\left[\frac{m_0 - m(t)}{V(t)}\right] \tag{4}$$

where c_b is the concentration of nanoparticles in the heart chamber, m_0 is the initial mass of nanoparticles injected, $V(t)$ is the time-dependent blood volume of the heart chamber, and $m(t)$ is the resulting sum of a volume integral of concentration over the tissue domain, computed in COMSOL. The partition coefficient K was further used to account for the discontinuity in concentration between the lumen and tissue sides of the boundary.

2) **At the boundary $\boldsymbol{r = r_3}$**, an aqueous semi-infinite approximation was implemented to model the diffusive behavior within the pericardial cavity. This physical approximation of the environment surrounding the cardiac tissue was based on a fundamental understanding of the physiology of the embryo during early stages of development. As a result, the following boundary condition was utilized,

$$-\frac{dc_a}{dr}(r = r_3) = 0 \tag{5}$$

5.5 Initial Conditions

At the beginning of the simulation, all tissues had a zero concentration of nanoparticles. It was assumed that immediately following injection into the yolk, the blood circulation became instantly

homogenized at a uniform concentration c_i, which was a function of m_0 and the fraction of total blood volume contained within the heart.

6. Experimental Analysis

In order to quantify the information stored within the micro-CT imaging data, an experimental method was developed that correlated the brightness of the images with the concentration of nanoparticles in the domain of interest. This quantification of the data was utilized in COMSOL to determine how diffusivity impacted the accumulation of mass in the tissue compared to *in vivo* observations. A process flow summarizing the steps in this analysis is provided in Figure 3.

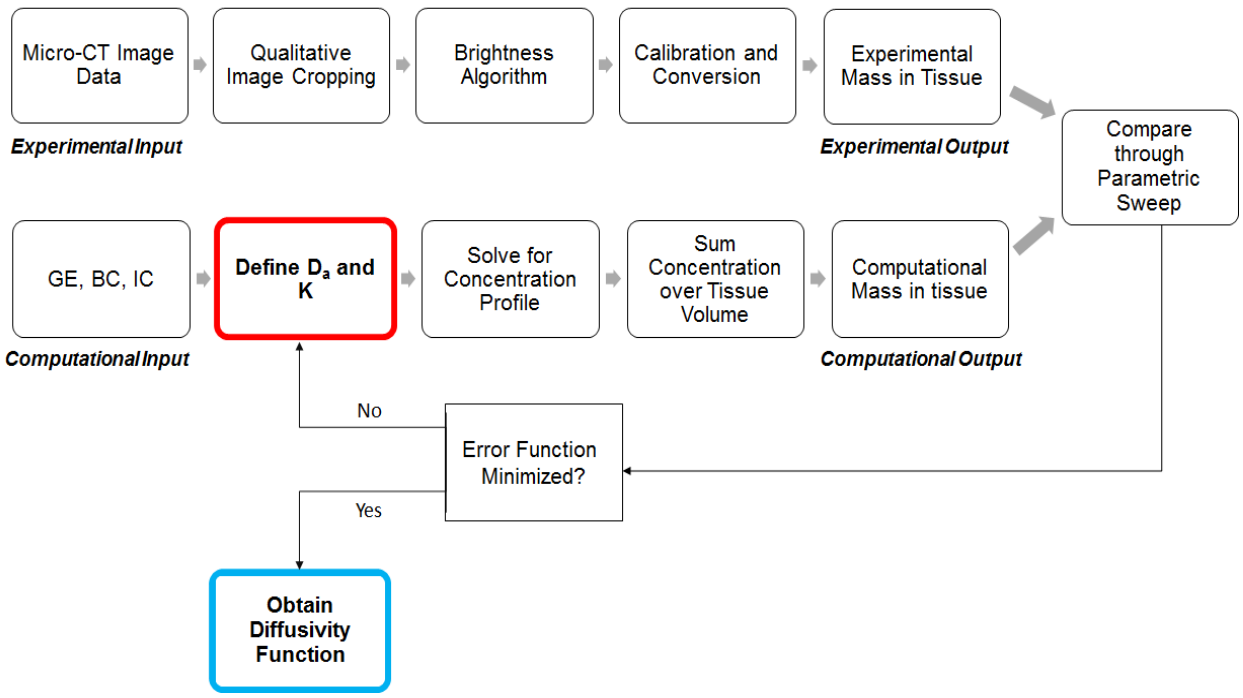

Figure 3. *Process flow diagram summarizing the experimental and computational analyses.*
Shown above is a simplified overview of the steps taken to generate experimental and computational mass values in the myocardial tissue to use in a comparative analysis. The details of each step are elaborated upon in the following section.

6.1 Image Data and Cropping

In order to acquire relevant concentration data from the micro-CT images, experimental analysis involving ImageJ DICOM manipulation was implemented for images captured at 2, 8, and 24 hour time points. We first selected the image slices that contained the chick heart and disregarded all other frames that were recorded from experimentation. A qualitative assessment was made for each DICOM frame to assess which portions of each image corresponded to myocardial tissue. The free-hand crop tool from ImageJ was then implemented to crop the pixels containing the heart to be used for subsequent image analysis. Note that brightness refers to a greyscale value between

0 and 65535 that MATLAB can store in a matrix element for each pixel of an ImageJ file. Next, we obtained calibration images of known masses of nanoparticles. These images were run through a MATLAB Brightness algorithm (see section 6.2) to generate brightness values from associated mass values. The code used to generate this algorithm is provided in Appendix C.

6.2 Brightness Algorithm

In order to generate discrete brightness values for each image, we wrote an algorithm in MATLAB to take an image or set of images as input and find a numerical sum of the brightness value over all the pixels; this would allow us to correlate the brightness in the images to nanoparticle mass in the tissue. A summary of the steps in the algorithm utilized for this purpose is summarized as follows, beginning with cropped micro-CT images from experiment:

1) Locate folder containing cropped micro-CT images
2) Store a single cropped image as an array of pixels in MATLAB
3) Subtract brightness noise value from each pixel to normalize against empty space
4) Sum brightness value for all elements in array
5) Store brightness sum for cropped image, then return to image directory
6) Repeat steps 2-5 until all images comprising the 3-D scan are processed
7) Sum brightness totals for all image slices into a total brightness for the 3-D scan

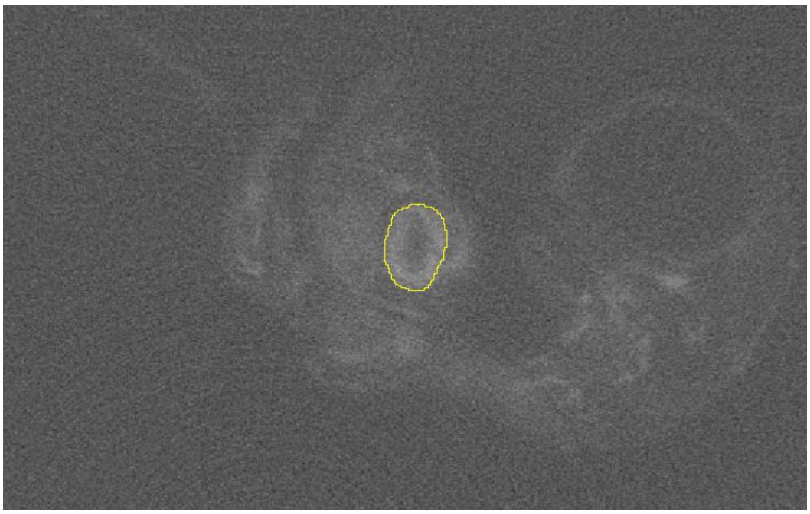

Figure 4. *Sample Process for Extracting Mass Values from Micro-CT Imaging Data (24hr).* The location of heart is identified in this particular DICOM frame, and a free-hand crop tool in ImageJ is used to isolate this tissue for use in the brightness algorithm.

These experimental steps, using the original selection of the heart for each DICOM frame, thusly determined the mass of nanoparticles that are in the myocardial tissue domain for use in comparison to our 1D diffusion model.

6.3 Calibration and Conversion to Mass

Once brightness values were obtained from the aforementioned algorithm, this information was next converted to a mass-equivalent description of the nanoparticle distribution so that a reliable comparison to the injection mass could be executed. To complete this conversion, a calibration curve was created using a standard dilution series of the nanoparticle contrast agent with a known mass being observed with micro-CT. From these standard images, the total brightness was obtained for each dilution of the original loading control, such that a linear relation could be derived. The resulting curve and regression are shown below in Figure 5. Note that a blank image was used as a zero baseline to normalize subsequent brightness values as well as to force the regression through the origin.

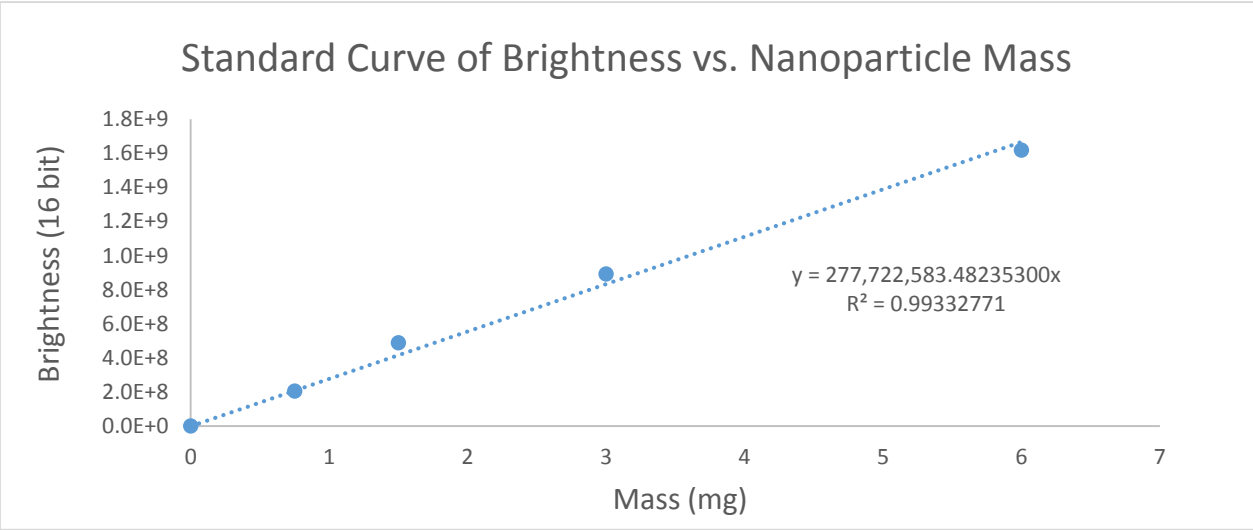

Figure 5. *Standardized curve for fitting nanoparticle mass to image brightness.* A calibration curve was created using a dilution series and blank images to correlate brightness values obtained from micro-CT images with corresponding mass quantities of nanoparticles used to generate these images.

7. Results

7.1 Image Analysis

After processing image data for all available time points, the change in mass in the tissue over time was determined, and the result is summarized in Figure 6, found below.

Figure 6. *Removed for the time being until work is published*

These set of points show a time-dependent decrease in the rate of accumulation of nanoparticle mass in the myocardial tissue, which was expected for the biological context of the simulation. Although these mass values were heavily dependent on how the images were cropped, a sensitivity analysis of the image processing method showed that there was very little variation between how each person cropped the tissue (Figure 8).

7.2 Solution

To calculate the mass in the tissue at a given time point, a volume integral of concentration over the domain was used. The masses at time points t = [2,8,24] hours will be compared with the masses from the experimental data at those time points. It is assumed that the initial mass in the tissue is zero. Unfortunately, experimental data was not available to confirm that this was actually the case, but given the dynamics observed so far, this is not an unreasonable assumption. A parametric sweep will be used to minimize the difference between the experimental mass and the mass from the model at both time points (see Section 7.4). This will help determine the diffusivity of the tissue at a given time point. Using the optimized values of A, B, K, the following concentration profile of nanoparticles was obtained.

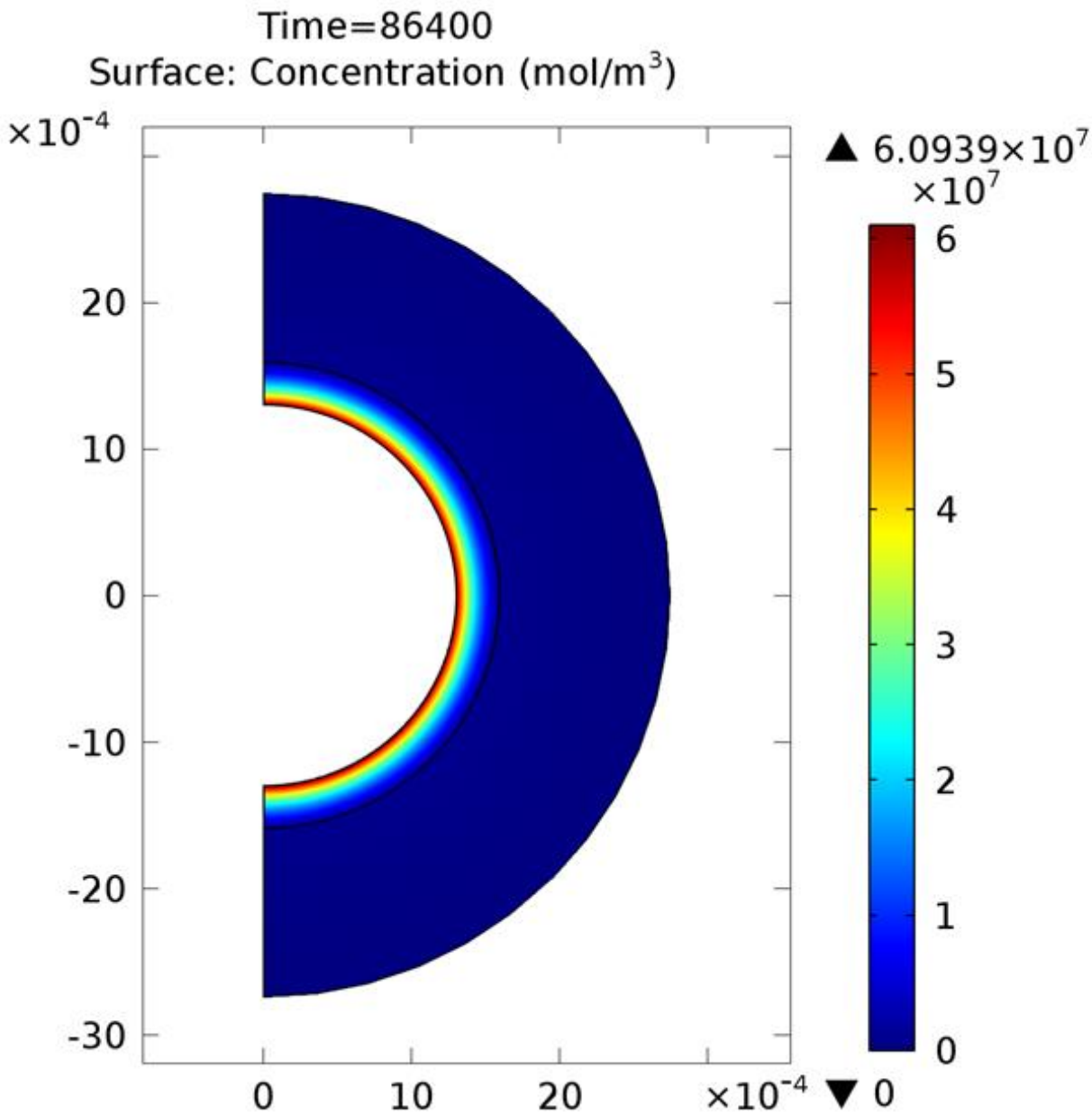

Figure 7. This figure shows the concentration profile of the nanoparticles within the heart tissue and Aqueous pericardial cavity at 24 hours. The black indicates the two distinct layers.

7.3 Sensitivity Analysis of Images and Computational Parameters

A qualitative sensitivity analysis was conducted to evaluate the responsiveness of computed mass values to the team's image cropping protocol. Because the extent of the image manipulation determined the level of brightness recorded by the computational algorithm, it was imperative that an understanding of the responsiveness of the brightness value to image processing be elucidated.

To accomplish this, an arbitrary subset of 10 image frames were selected to be processed independently by three different operators, and the resulting brightness and mass values were obtained for each subset. The images from the 24 hour data were selected for this analysis because they were the most consistent and easily visible among the time points, allowing the group to focus in on the operator's specific cropping methods and not the ambiguity generated by the image itself. The total mass recorded by each operator is displayed in Figure 8, along with the average mass recorded for all three subsets processed.

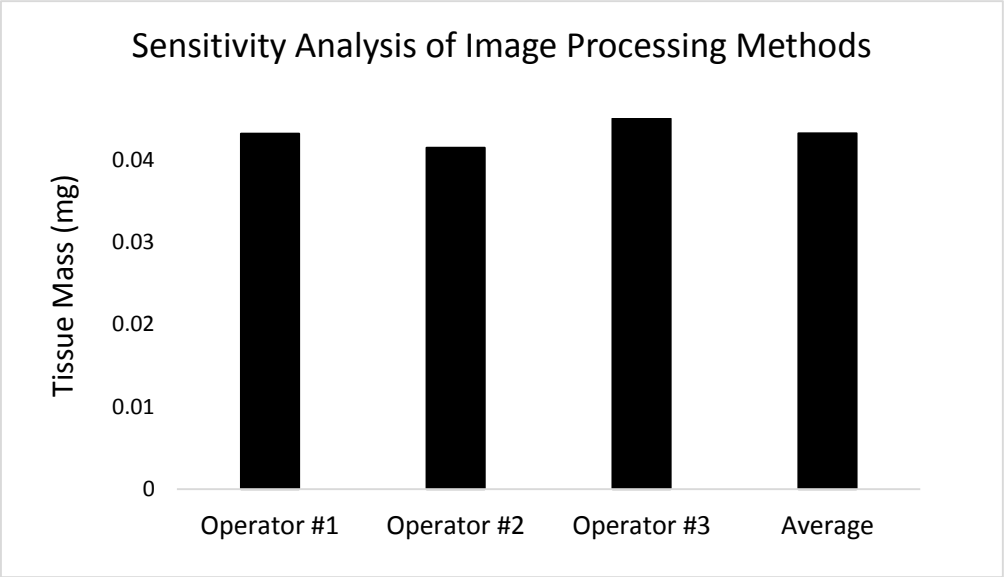

Figure 8. *Sensitivity Analysis of Image Processing Methods*. Shown above are the results of a qualitative sensitivity analysis conducted to assess the impact of image manipulation technique on the resulting tissue mass values computed from micro-CT image analysis.

The average tissue mass recorded from these 10 frames was 0.0432 mg, with a minimum and maximum value of .0415 mg and .0451 mg, respectively. Operators #2 and #3 produced mass values that only deviated less than approximately 4.1% from the mean mass value recorded, while Operator #1 produced a mass value nearly identical to the average. This suggests that the computed mass was not extensively sensitive to slight nuisances in the operators' image manipulation methods. One of the frames from this analysis was selected to qualitatively identify differences in processing methods that might pose a problem in analysis, and these images are presented below in Figure 9.

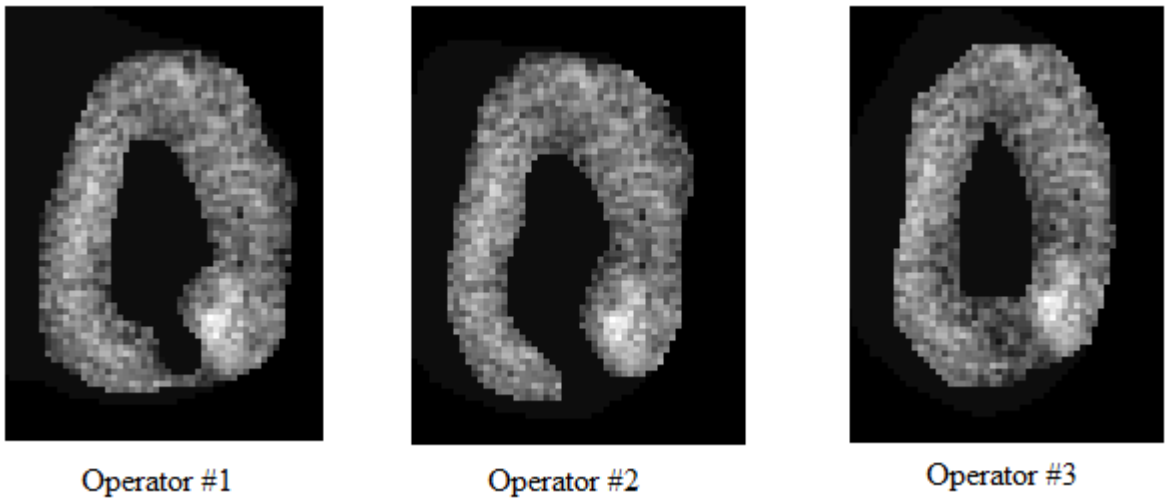

Figure 9. *Sample Images from Operators in Sensitivity Analysis.* Shown above is an image selected from the 24 hour micro-CT data that was processed individually and independently by three different operators. Small differences in pixels that have been included in the processed image can be seen among operators, indicating slight variations in method that impacted resulting mass calculations.

These images presented a clear outline of the myocardial tissue, with two segmentations indicating what appears to be two different ventricles within the heart. Although the particular image used in the sensitivity analysis was somewhat arbitrary, it was clear that certain qualitative differences between the techniques used by each operator would invariably affect the actual data processing.

After conducting our optimization to find the computational parameters A, B, and K, we performed a sensitivity analysis by fixing two of the parameters and allowing the other to vary. This was done for each of the three parameters and the following data was gathered.

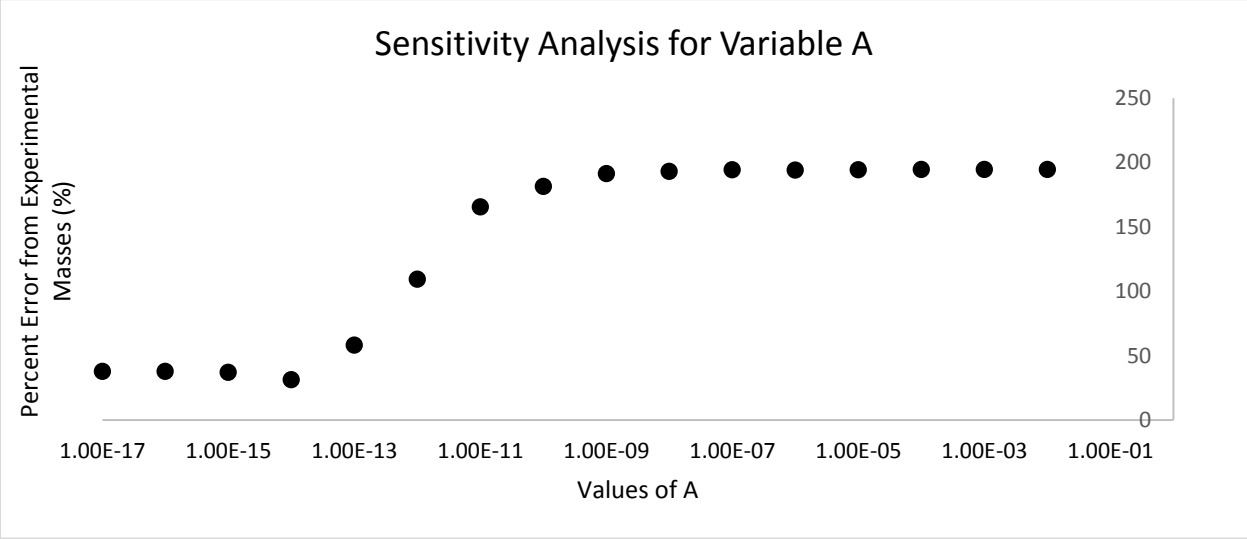

Figure 10. *Sensitivity Analysis for Variable A.* This graph shows that the minimum amount of error was when A = 10E-14.

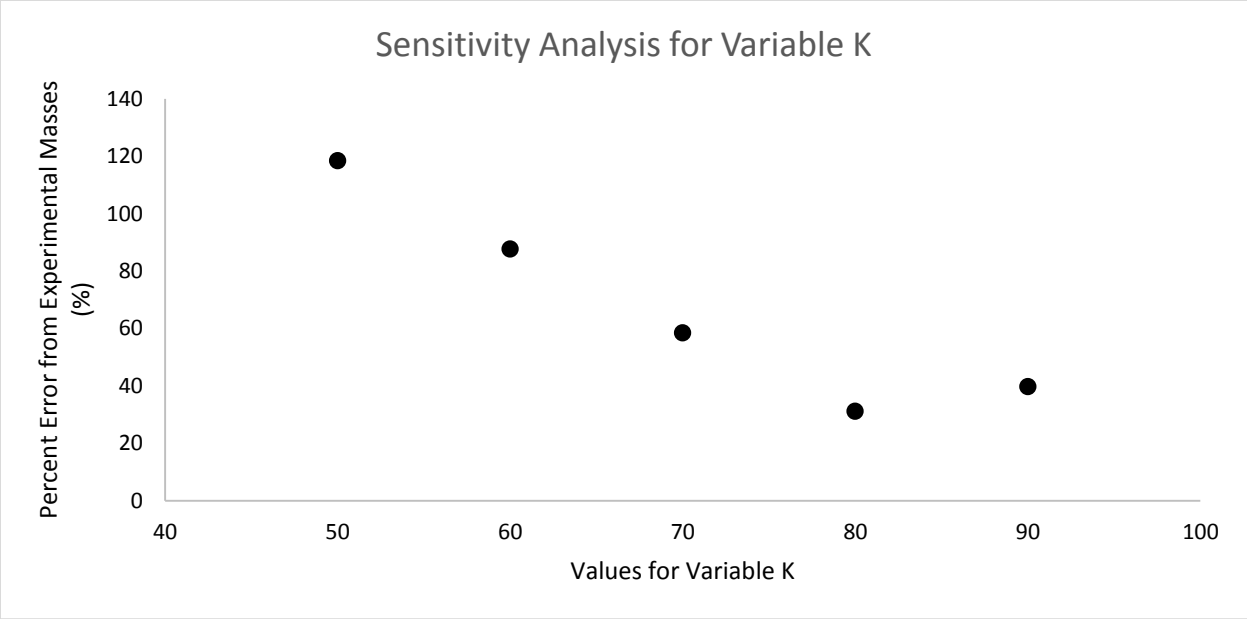

Figure 11. *2Sensitivity Analysis for Variable K.* This graph shows that the minimum amount of error was when K = 80

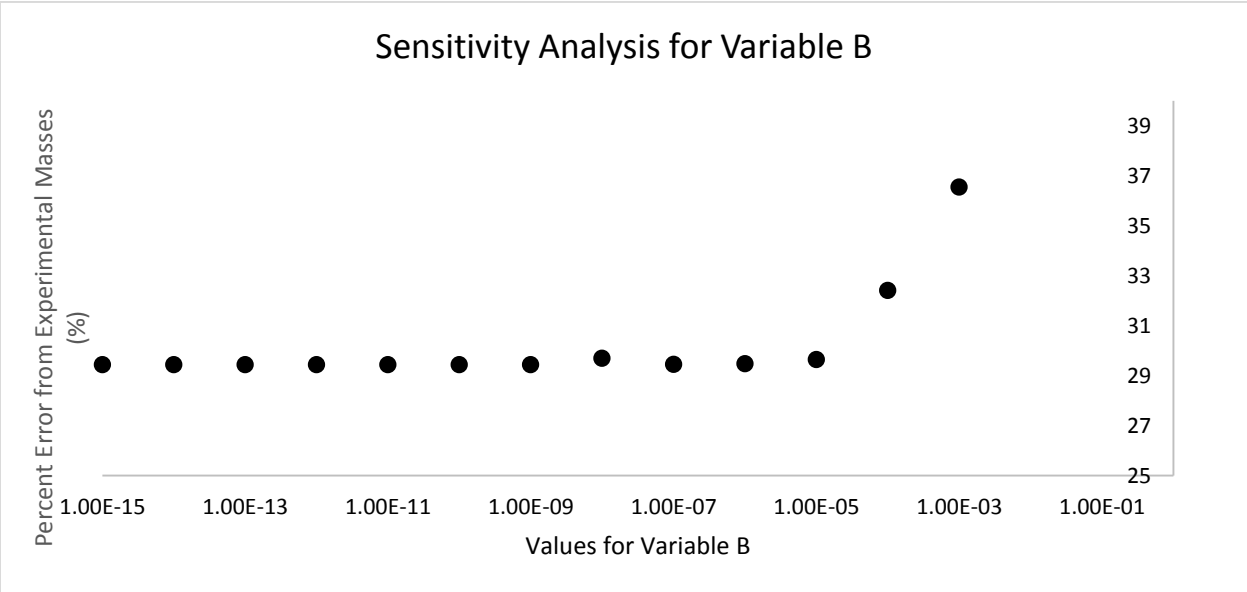

Figure 12 *Sensitivity Analysis for Variable B.* This graph shows that the minimum amount of error was when B = 10E-7.

From our findings, it was clear that changing parameter B had the least amount of effect on the percentage error in our model. Both Parameters A and K significantly affected the percentage error in our model.

7.4 Optimization

In our optimization process, we used the error function in Equation (6) to analyze the difference between the experimental mass and model mass at each time point, normalized by the experimental mass.

$$\sum_{i=1}^{3} \frac{|Experimental\ Mass(t_i) - Model\ Mass\ (t_i)|}{Experimental\ Mass(t_i)} \tag{6}$$

The impact of the computational parameters A, B, and K on the overall computational solution were analyzed using a parametric sweep, and the values that minimized the error function produced the blue dotted line in Figure 10 below.

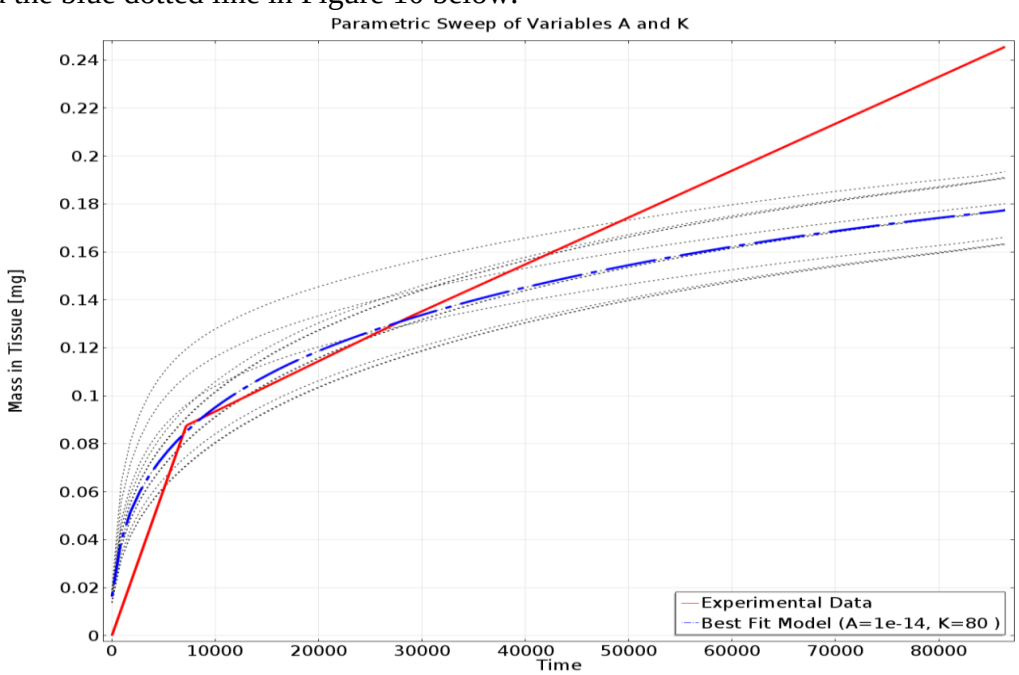

Figure 13. Comparison of Experimental Data, in red, with a parametric sweep of computational variables, in black. Blue-dotted line is the computational solution that yields the smallest error function.

The diffusivity function and partition coefficient values that produce the best-fit solution are seen below.

A= 10E-14, B=10E-7, K = 80

$$D_a = 1.0 * 10^{-14} e^{-10^{-7} t} \quad , \ K = 80 \tag{7}$$

8. Conclusions

8.1 Implications

Based on the extensive image analysis conducted during this project, it was first concluded that micro-CT images could be used to consistently obtain a precise and real-time quantification of nanoparticle tissues in embryonic tissue. These images showed accumulation of the nanoparticle in the myocardial tissue. Furthermore, they showed a decrease in the rate of accumulation over time. Both of these results were consistent with our expectations, because gold nanoparticles are readily diffusible, and because the concentration gradient decreases with diffusion of the particles into the tissue.

Although the sensitivity analysis of the image processing method showed high fidelity, the COMSOL model did not completely fit the experimental results. While the model matched the experimental values very well at early time points, it consistently underestimated the mass in the tissue at 24 hours. This could have been attributed to an error in the diffusivity function; perhaps an exponential decay function was not the most appropriate function.

This need to improve the COMSOL model could be seen throughout. Based on the sensitivity analysis of B, the value of B had little impact on the overall mass profile for the computational model, as long as the order of magnitude of this value was less than or equal to $10^{-3}\,s^{-1}$. This showed little dependence of the results on the exponential nature of the diffusivity function. Furthermore, the incorporation of a partition coefficient improved the minimization of error during computational analysis, suggesting that there may have been some form of hydrophilic interaction between nanoparticles and the blood within the lumen of the heart, causing a discontinuity in the concentration profile across this boundary. Clearly, there were interactions with the nanoparticle that the current model did not take into account.

8.2 Design Constraints

Though the extent of the modeling work described above was quite productive, there were several important limitations that were placed on the entire project that prevented a holistic understanding of the dynamics of chick embryology. The assumptions made in the model design notwithstanding, inaccessibility to additional data also prevented the group from effectively simulating diffusion in organs other than the heart. Specifically, it was difficult to discern the tissue corresponding to other organs for the time points available, mainly because the vascularity was not developed enough in these organs by day 8 to provide reliable information from the micro-CT images. What is more, only a few time points were available for analysis, making the optimization process relatively coarse compared to a continuous set of micro-CT imaging data. In reality, it was difficult to determine how well the diffusivity function described the properties of the myocardial tissue

simply because a large amount of interpolation was needed to approximate the behavior between available time points.

In terms of the computational model, many of the simplifications made prevent it from accurately depicting the nanoparticle diffusion. For example, isolating the heart from the rest of the tissue neglected the diffusion of the nanoparticles from the blood into other parts of the body. It was clear that this occurred, as various parts of the body are illuminated at 24 hours. In addition, the diffusivity function was assumed to be spatially constant in the heart tissue while varying temporally. Although the heart tissue was quite thin, this simplification neglected the variable differentiation within myocardial tissue. Finally, the heart was approximated as a sphere. Clearly, this was not the case, as can be seen in the Micro-CT images. A 3-D image would have yielded a much more realistic geometry.

8.3 Design Recommendations

In retrospect, it became evident *in vivo* images are often subject to incredible variability, making it difficult to draw quantitative conclusions from such experimental data. Moving forward with this work, it was advised that efforts be made to obtain a more continuous set of time-dependent experimental data to create a more robust mass function for comparison to a computational model. While speculation was possible about the change in diffusivity over time, more fruitful discussion would have been possible with access to additional data from additional time points within the 24 hour period. Furthermore, both the context and geometry of the computational model limited the scope of this project to a simplified diffusion simulation of the myocardium. Moving forward, it would be invaluable to incorporate the movement of nanoparticles between multiple organs, using a compartment model to more readily capture the actual transport of nanoparticles within the embryo. This would require additional information about the tissue as well as a more in-depth analysis of the micro-CT images as a whole. Furthermore, based on the differences between the experimental and computed mass values, a different diffusivity function should be used. Moreover, while mass accumulation was studied in this project, the actual distribution of nanoparticles was neglected for computational analysis. It was possible that the methods used in this project could be extended to resolve a 2D distribution of nanoparticles over time, which provide additional information to be referenced against the modeling capabilities in COMSOL.

9. Appendix A: Mathematical Statement of the Problem

Definitions:

Symbol	Definition	Value
r_1	*Inner chamber radius*	1.37 mm → 1.44 mm
r_2	*Outer myocardium radius*	1.45 mm → 1.59 mm
r_3	*Pericardial cavity radius*	3.18 mm
$v_i \quad (i = 1,2)$	*Boundary velocity*	$\frac{r_{i_{final}} - r_{i_{initial}}}{24\ hours}$
c_a	*Nanoparticle concentration*	From model
C_b	*Boundary concentration*	$C_b(t) = K\left[\frac{m_0 - m(t)}{V(t)}\right]$
D_a	*Diffusivity*	$D_a = Ae^{-Bt}$
A	*Diffusivity scalar factor*	10E-14
B	*Diffusivity exponent factor*	10E-7
K	*Partition coefficient*	80
m_0	*Injection mass*	.435 mg
m(t)	*Tissue mass*	From volume integral
V(t)	*Chamber volume*	Interpolated from literature

Governing Equation:

$$\frac{\partial c_a}{\partial t} = \frac{D_a(t)}{r^2}\frac{\partial}{\partial r}\left[r^2\frac{\partial c_a}{\partial r}\right]$$

Boundary Conditions:

At the boundary $r = r_1$: $\quad C_b(t) = K\left[\frac{m_0 - m(t)}{V(t)}\right]$

At the boundary $r = r_3$: $\quad -\frac{dc_a}{dr}(r = r_3) = 0$

Initial Conditions:

$$c_{all\ domains} = 0$$
$$m_{injected} = .435\ mg$$

Assumptions:

- Concentration of nanoparticles in systemic circulation is uniform
- Myocardium geometry simplified to a axisymmetric sphere
- Neglect diffusion dependences in φ or θ directions
- Neglect convective and derivative effects on concentration of nanoparticles
- Myocardial domains grow with a linear velocity
- System is constrained to a 24 hour period of simulation
- Semi-infinite condition at far-field locations within computational domain
- Diffusivity modeled as an exponential decay function over the duration of the simulation
- Initial concentration of lumen is equal to initial concentration in systemic circulation

10. Appendix B: Processed Experimental Data

Table B1. *Processed Values of Experimental Data for Calibration and Analysis*

Calibration Curve from Dilution Series		
Dilution (%)	Mass Dilution (mg)	Total Normalized Brightness (16-bit)
100	6	1.62E+09
50	3	8.93E+08
25	1.50	4.88E+08
12.5	0.75	2.06E+08
0	0	0
Mass Data from Experimental Images		
Time (hours)	Myocardial Tissue Brightness (16-bit)	Myocardial Tissue Mass (mg)
0	0.00	0
2	9.65E+07	0.0876
8	3.69E+07	0.1330
24	1.06E+08	0.2455
Initial Heart Lumen Parameters		
Inection Mass (mg)	Initial Heart Chamber Mass (mg)	Initial Heart Chamber Brightness (16-bit)
10.5	0.435	1.21E+08

11. Appendix C: Brightness Algorithm

A procedure was developed in MATLAB to systematically convert information stored in micro-CT images into quantitative mass data using the brightness values stored in each pixel of the images along with a calibration curve provided from experimentation. The MATLAB code used in processing these images is shown below, annotated for ease of access.

```
% BEE 4530: Computer-Aided Engineering
% Group 7
% Date Created: 2/3/15
% Date Modified: 5/6/15

% Brightness.m converts monochrome values stored in the pixels of micro-CT
% DICOM files into singular scalar representations of the total brightness
% in a given region of the micro-CT image. Additional conversions are
% completed separately to translate this information into a quantitation of
% the nanoparticle mass within the region of interest.

%% NOTE: All DICOM images were initially processed then saved as .PNG files.
%%

% Identify the directory and folder location of the files of interest:
D=what;
maindir=D.path;
folder_img='\FolderName\';

% Execute for loop to process each image individually:
for k=1:NumFiles % NumFiles is chosen based on operator's needs
     if k<10
         num=strcat('00',int2str(k)); % Standardized naming method of files
     elseif k >=10 && k<100
         num=strcat('0',int2str(k)); % Standardized naming method of files
     else
         num=int2str(k);
     end
    str=strcat('Slide',num); % Standardized naming method of files
    file=strcat(maindir,folder_img,str,'.png');

% Read each image file into MATLAB as an array of pixels:
M=imread(file);

% Subtract off noise associated with baseline brightness for .PNG files:
noise = 32768; % this noise comes from black space in the DICOM directly
N=M;
N=N-noise;

% Set minimum brightness to zero:
N(N<0)=0;

% Clean up array using 'salt & pepper' filtering method in MATLAB:
K=medfilt2(N);

% Sum brightness values from each pixel in image k:
Brightsum(k)= sum(sum(K)); % Store total brightness for each image in sequence
Total = sum(Brightsum); % Store total brightness over all images
end
```

12. Appendix D: Mesh & Mesh Convergence

Because our problem involved both the diffusion from the heart chamber into the myocardial tissue as well as diffusion from the tissue into the pericardial cavity (modeled as a quasi-aqueous domain), it was evident that changes in concentration would occur most rapidly at the boundaries between the domains. Consequently, it was necessary to formulate a mesh such that large numbers of nodes occur at these boundaries. This was achieved by using a physics-controlled mesh with a set maximum element size. Because the physics does not change with the moving boundaries, this mesh should adapt with the changing geometry without an increase in discretization error. The mesh for t=0 hr can be seen in the appendix (Fig. 14).

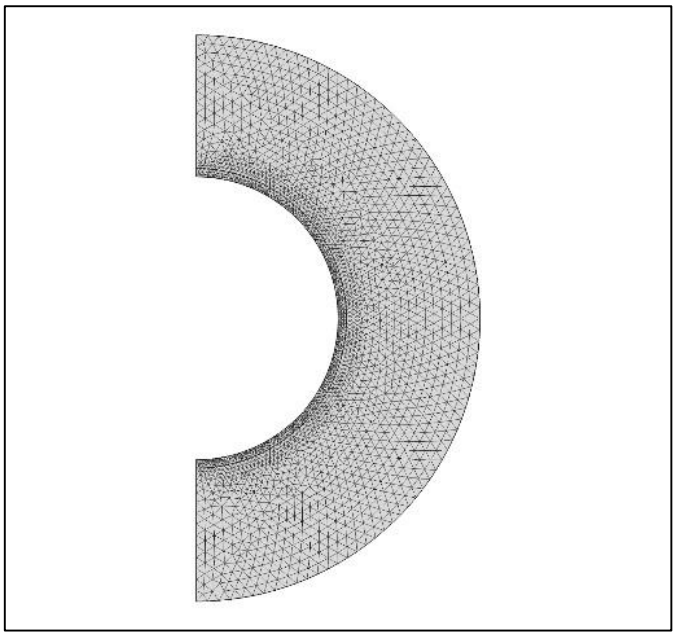

Figure 14. *Mesh utilized in obtaining preliminary solution.* Shown above is the structured mesh created for the geometry of our diffusion problem at t=0 (day 7). The boundary between the tissue and pseudo-aqueous domain occurs at $r=r_1+0.08$ mm. A physics-controlled mesh for a deformed geometry with an extra fine element size was used to yield the most elements near the boundaries.

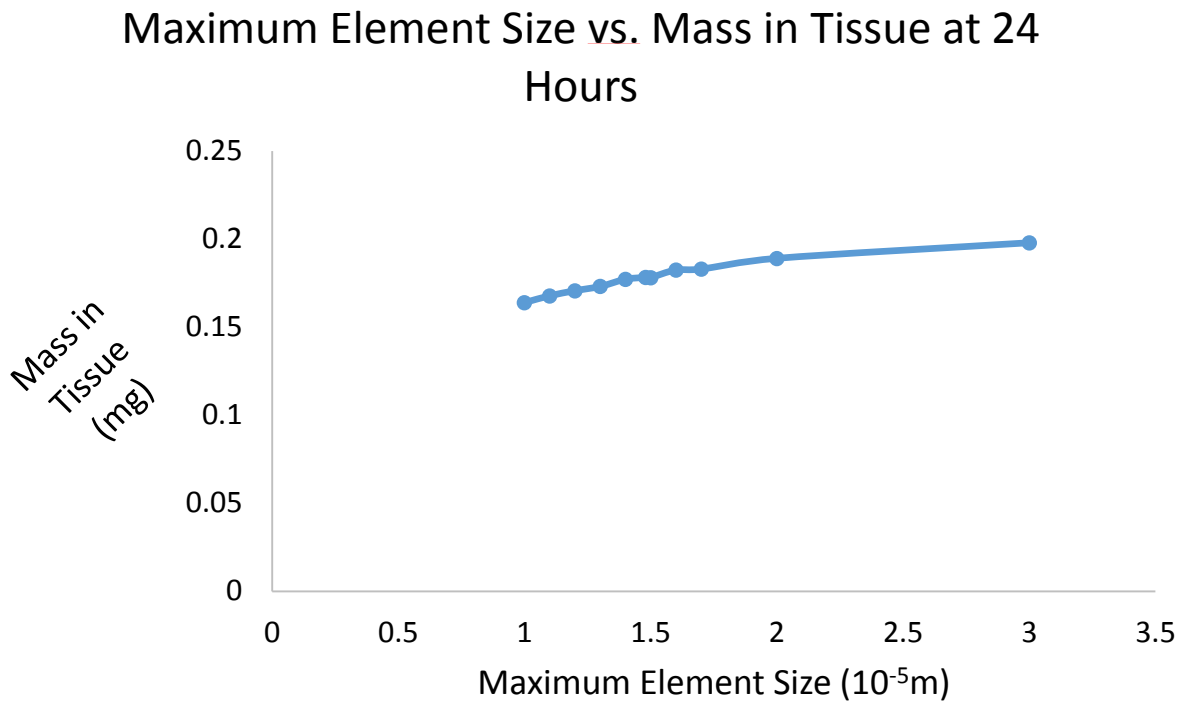

Figure 13: The graph above shows the relationship between the maximum element size and the mass in the tissue at the optimized values of A,B, and K.

By decreasing the Maximum Element Size (or increasing the number of nodes), the Mesh Convergence showed that the resulting mass values decrease slightly with higher amounts of nodes. This graph shows that the mesh does not adequately converge due to computational limitations that prevented us from analyzing finer meshes. This may be due in part to the large amount of computation necessary to create the mesh given the moving boundary phenomena implemented in the model. In order to account for this, we acknowledge that the COMSOL model may have slightly overestimated the tissue mass, which would have been accounted for had we been able to compute using finer meshes.

13. Appendix E: References

1. Gregg, Chelsea L., and Jonathan T. Butcher. "Quantitative in vivo imaging of embryonic development: opportunities and challenges." *Differentiation* 84.1 (2012): 149-162.

2. Mercker, Moritz, Dirk Hartmann, and Anna Marciniak-Czochra. "A Mechanochemical Model for Embryonic Pattern Formation: Coupling Tissue Mechanics and Morphogen Expression." *PloS one* 8.12 (2013): e82617.

3. Hu, Norman, and E. B. Clark. "Hemodynamics of the stage 12 to stage 29 chick embryo." *Circulation Research* 65.6 (1989): 1665-1670.

4. Butcher, Jonathan T., et al. "Quantitative volumetric analysis of cardiac morphogenesis assessed through micro-computed tomography." *Developmental Dynamics* 236.3 (2007): 802-809.

5. Kim, Jun Sup, et al. "Quantitative Three-Dimensional Analysis of Embryonic Chick Morphogenesis via Microcomputed Tomography." *The Anatomical Record* 294.1 (2011): 1-10.

6. Murphy, Catherine J., et al. "Gold nanoparticles in biology: beyond toxicity to cellular imaging." *Accounts of Chemical Research* 41.12 (2008): 1721-1730.

7. Hamburger, Viktor, and Howard L. Hamilton. "A series of normal stages in the development of the chick embryo." *Journal of morphology* 88.1 (1951): 49-92.

8. DeHaan, Robert L., and James D. Ebert. "Morphogenesis." *Annual review of physiology* 26.1 (1964): 15-46.